2018 European Control Conference (ECC)
June 12-15, 2018. Limassol, Cyprus

Droplet Observer for Pulsed Gas Metal Arc Welding

K.M. Nielsen[1], T.S. Pedersen[1] and S. K. Ovedahl[1,2]

***Abstract*— In this paper an observer for detecting droplet detachment/no-detachment for a pulsed gas metal arc welding (GMAW) is developed. The observer is based on simple calculations made on the measured welding apparatus voltage. Two phenomena are used in the observer, one is the shape of the voltage in a limited time interval and the other is detection of a potential spike in the voltage. The observer is implemented on a Migatronic embedded welding computer and tested on-line on a welding. The observed droplet detachment is compared with photos from a high speed camera showing good results. One use of the droplet observer is to automatically adjust the pulse current level to obtain a proper welding. This controller is tested and able to achieve an appropriate welding current.**

I. INTRODUCTION

Gas Metal Arc Welding (GMAW) is a process used for joining pieces of metal; this is probably the most widely used welding method in industry. In the welding process the consumable electrode is heated to the point of melting turning it into a molten droplet that is transferred to a weld pool. This can be done in different ways, the most common being short arc GMAW and spray mode GMAW. In this paper a subclass of the spray mode GMAW called pulsed GMAW detaching one droplet per pulse is investigated. In this welding a current pulse detaches a droplet. The shape of this current pulse intend to detach one and only one droplet per pulse without making spatter and keeping a sufficient low temperature in the welding pool.

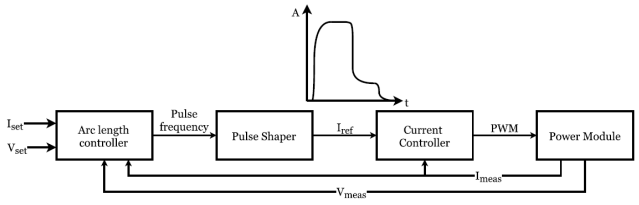

Fig. 1. Control concept for pulsed GMAW welding.

In Fig 1 the welding control system is shown. The frequency of the pulses are determined by the 'Arc length controller' and the 'Pulse Shaper' giving the current reference, I_{ref}. A controller makes the welding current follow the reference current by adjusting the output voltage from the welding machine. The I_{ref} can be shaped depending on the welding thread and the workpiece. I_{ref} consists of different parts where each part can shift level and time duration.

[1]Institute of Electronic Systems, Automation and Control, Aalborg University, Aalborg, Denmark kmn,tom@es.aau.dk
[2]Now at Migatronic A/S, Denmark sko@Migatronic.dk

If the I_{ref} is not perfectly fitted to the welding thread and the workpiece there is not a one-to-one relation between droplets and pulses, meaning that there may be pulses that do not detach droplets. This results in spatter. In the existing system I_{ref} is manually set based on information on materials. On-line detection of the droplet is very difficult as the only measurable signal is the welding voltage U_m. Droplets can be identified using a high speed camera, this is though not well suited for practical implementation. The purpose of this work is to observe detachment of droplets from the voltage signal U_m and based on that to adjust I_{ref} for better performance.

Measurements indicates that the shape of U_m for individual pulses differs even for pulses with droplet detachment; this is also the case for pulses with no droplet detachment.

Droplet detection could be based on data driven methods like e.g. neural networks trained from detach/no detach based on pictures from a high speed camera in combination with the reference signal I_{ref} and the measured welding voltage U_m. This is difficult and results in a complex neural network as I_{ref} may have varying shapes, because I_{ref} is on-line adjusted by the 'Pulse Shaper'. A second possibility is to include knowledge using a model. One way to do this is to use Kalman filters in combination with a hypothesis test. This method is heavily computable and combined with a 50 k Hz sample frequency it is not well suited for implementation in an embedded welding computer. A third method is to make a thorough inspection of the voltage signal U_m combined with high speed camera pictures and physical welding knowledge to obtain U_m characteristics for detach/ not detach of droplets. If these characteristics are possible to identify and simple to recognise solely based on U_m the later method is preferable as it might be simple to implement. This method is in focus in this paper.

A voltage pulse shape can be seen at figure 6. The droplet should be detached between T_4 and T_{end}. It is assumed that droplet detachment/non-detachment influences the present and the succeeding U_m shape. It may be a characteristic in the first part of a shape, in the figure from T_{end} and forward, that tells whether there has been a detachment in the previous pulse. Another potential characteristic could be found in the end of the present shape, between T_4 and T_{end}. For control purposes an early detection is preferable. In this work an on-off on-line observer is developed and implemented in an automatic welding parameter adjustment controller showing signs of future success. The concept is tested on particular welding thread.

In section II the test set-up is described, section III describes the model used in a welding simulator, section

IV gives the details in the droplet detachment observer. The test results for the observer is in section V, section VI is automatic welding parameter adjustment based on the observer and finally section VII is the conclusion.

II. DESCRIPTION OF THE TEST SET-UP

Fig. 2. Laboratory test set-up at Migatronic A/S.

A test set-up is placed at Migatronic A/S. It consists of a Migatronic Sigma GALAXY 500 Robo welding machine, a Fanue ARC Mate 100iC welding robot, a Fastcam Mini UX100 high speed camera and Migatronic's embedded welding computer. This test set-up makes it possible to measure time correlated voltages, currents and photo's. The set-up is used for model analysis as well as final controller tests.

III. MODELLING OF PULSED GAS METAL ARC WELDING

Dynamic models of GMAW may be found in [1], [3], [4], [5], [6], [7], [8] and [9]. A simulation tool based on these models has been developed in a collaboration between Migatronic A/S and Aalborg University, [2], making it possible to relate time series of U_m and I_{ref} to physical welding behaviour.

In Fig. 3 the components and some of the variables used in the modelling are shown. The system consists of the welding machine, the wire system, the electrode, the droplet and the workpiece. The model consists of the following parts: the electrical system, the droplet dynamics, the electrode energy system and the droplet detachment part. To make the model description short some of the lengths, volumes, densities etc. are omitted in the representation. A brief description of the models are presented. For the full model see [2].

Electrical system

The electrical system consists of a wire model described by resistances and inductances, an electrode model which consists of a non-linear resistance which is dependent on

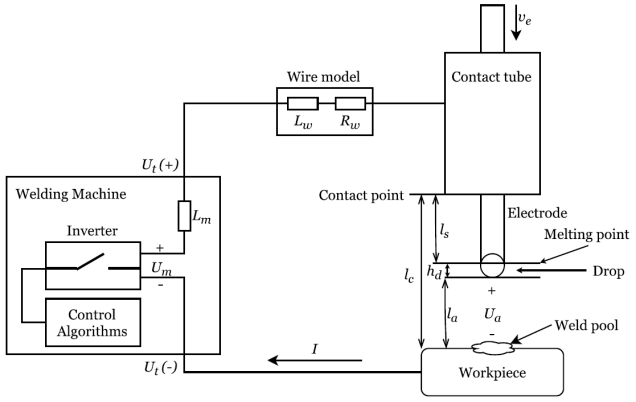

Fig. 3. The welding system, components and the model notation.

the length and resistivity of the stick out, l_s in Fig. 3. The resistance in the droplet is dependent of the volume. The final element is the arc voltage, U_a.

$$U_m(t) = (L_m + L_w)\dot{I}(t) + (R_w + R_e(t))I(t) + U_a(t) \quad (1)$$

where I, L_m, L_w, R_w, U_a appear from Fig. 3. R_e is the sum of electrode and droplet resistances.

Droplet dynamics

The droplet is affected by gravity force, F_g, electromagnetic force, F_{em}, and tension force represented by a spring force, $k_d x_d$ and a damper force $b_d \dot{x}_d$

$$F_{em}(t) + F_g(t) - b_d\dot{x}_d(t) - k_d x_d(t) = m_d(t)\ddot{x}_d(t) \quad (2)$$

where x_d is the position of the droplet. Note that the drop mass, m_d, is time dependent.

Electrode energy model

From the contact point to the droplet power is added to the electrode. The temperature increases until the melting point is reached and a drop is formed at the end of the electrode. The drop volume increases until the drop is detached.

The solid part of the electrode is modelled using distributed parameters resulting in a partial differential equation. This equation is solved by lumping it in five sections. The equations can be seen in [2].

The droplet is modelled by an energy balance given by

$$\frac{d(V_d(t)H_d(t))}{dt} = P_{da}(t) + P_{dJ}(t) + P_{dc}(t) - H_d(t)M_R(t) \quad (3)$$

where V_d is the droplet volume, H_d heat content of the droplet, P_{da} is the heat from the arc, P_{dJ} is the power from the electrical current, P_{dc} is heat from the electrode and M_R is the melting rate.

Final model without detachment criteria

The final model consists of 10 non-linear differential equations. After parameter fitting the output of the model and corresponding measurements can be seen in Fig. 4; here there is droplet detachment for all pulses. As seen there is a fair relation between the model and the measurements.

An important model feature is to detect detachment, as described in the next subsection; here at least two different model approaches are used.

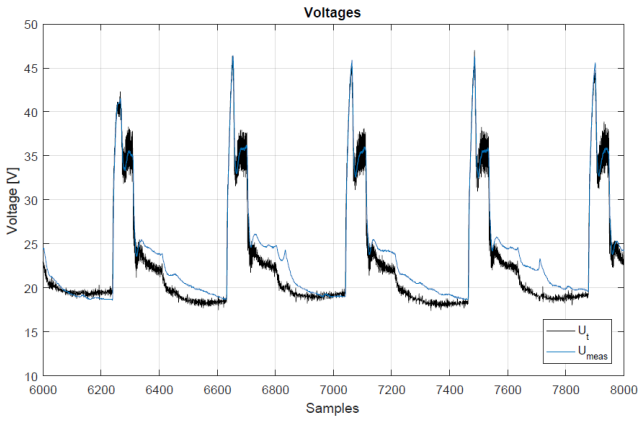

Fig. 4. Output of model and measurements. For all the shown pulses drop detachment takes place (seen at the high speed camera).

Detachment

In litterature , [6], detachment of droplets can be expressed using the droplet radius or by the downward drop-forces acting on the drop and a maximum surface tension.

Using the radius criteria the droplet radius r_d, see Fig. 5 is compare to a certain critical radius r_{dc}, [6].

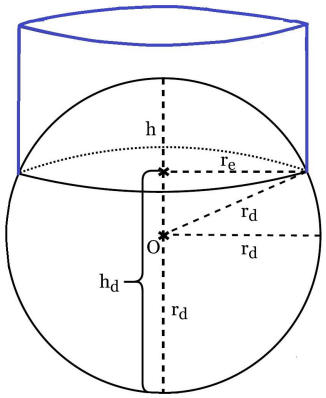

Fig. 5. Ideal droplet geometry. The electrode (blue) is in the top of the droplet with radius r_e.

$$\text{Detachment if:} \quad r_d(t) > r_{dc}(t) \tag{4}$$

$$\text{where } r_{dc}(t) = \frac{\pi(r_d(t)+r_e)}{1.25(\frac{x_d(t)+r_d(t)}{r_d(t)})(1+\frac{\mu_o I(t)^2}{2\pi^2\gamma(r_d(t)+r_e)})^{\frac{1}{2}}}$$

r_e is the electrode radius, see Fig. 5, γ, μ_o are constants, x_d is the droplet position described in the droplet dynamic section.

Another detachment criteria is to compare the total downward drop-forces acting on the drop F_{total} and a maximum surface tension force F_s, [6].

$$\text{Detachment if:} \quad F_{total}(t) > F_s(t) \tag{5}$$

The two criteria are frequently used in literature, though in [2] neither of these detachment criteria give a good match with the measurements.

IV. DROPLET DETACHMENT OBSERVER

The intended use of the model was to make a droplet detachment observer in a Kalman filter framework. A Kalman filter based on the model described in section III, is computationally heavy therefore the idea was to simplify this for implementation. During this work the voltage signal and the current signals were thoroughly examined. A pattern in the voltage signal related to detachment/no-detachment of the droplet was recognized. This pattern is shown in Fig. 6.

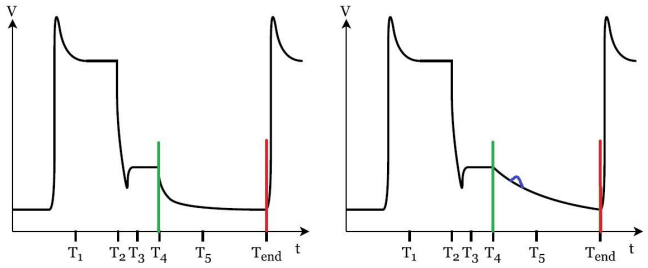

Fig. 6. Sketch of voltage U_m. Detachment (left)/No-detachment (right). A voltage spike (blue) is shown on the right plot, this spike occurs rarely and indicates detachment even though the curvature indicates no- detachment.

From time T_4 to time T_{end} there is a difference in the curvature depending on droplet detachment. In the right sketch the voltage is approximately a straight line, whereas the voltage in the left plot is more curved. In the laboratory synchronized measurements of the voltage U_m and pictures of the welding are recorded. A subset of the measurements is shown in Fig. 8 where sequences with detachment are black and no-detachment are red. A straight line starting at time T_4 to time T_{end} is added to make clear the different curvatures.

The physics behind the difference are explained using simulation in Fig. 7.

In Fig. 7 the green vertical lines indicate the times T_4 and the red lines are at T_{end}. It is assumed that the melting rate is constant. After detachment a new droplet has a small r_d which will imply a fast growth of h_d, as the droplet radius r_d reaches its max value (steady state), the increment of the height h_d is almost linear. An un-detached droplet will imply an almost linear growth of h_d in the entire interval from T_4 to T_end , since the radius is nearly constant in this situation. This is observed at Fig. 7. In interval b,d,e,f,g and i the droplet is detached, in a,c and h there is no detachment.

The observer calculates detachment by making a cross-correlation between a straight line and the curve from T_4 to T_{end}. Note that the time interval from T_4 to T_{end} is varying. The straight line is fixated in the two end-points by $(T_4, U_m(T_4))$ and $(T_{end}, U_m(T_{end}))$, and described by

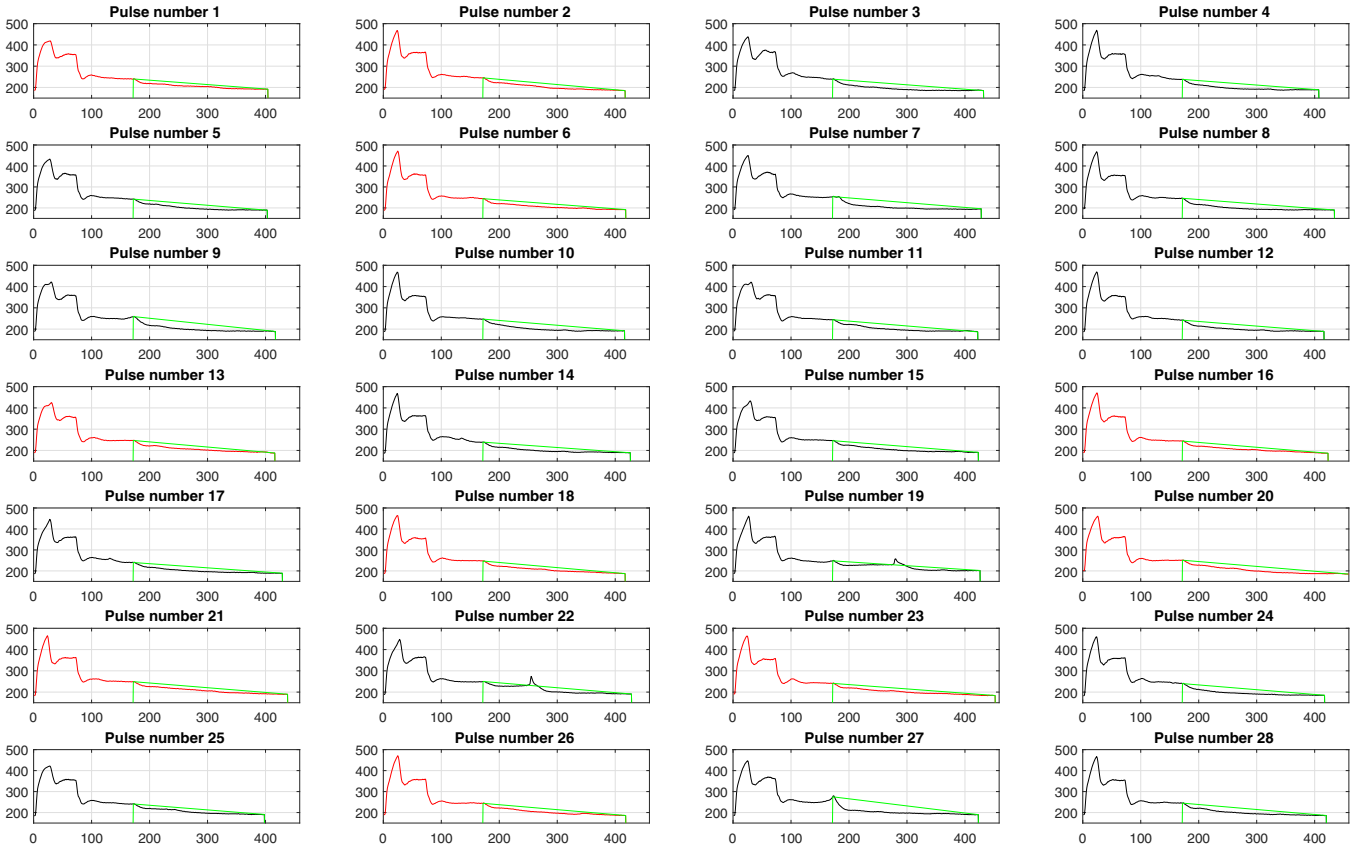

Fig. 8. Test results from the laboratory set-up of U_m. The y-axis on all plots are in volt multiplied by 10. The x-axis is samples. There is no droplet detachment in the red curves.

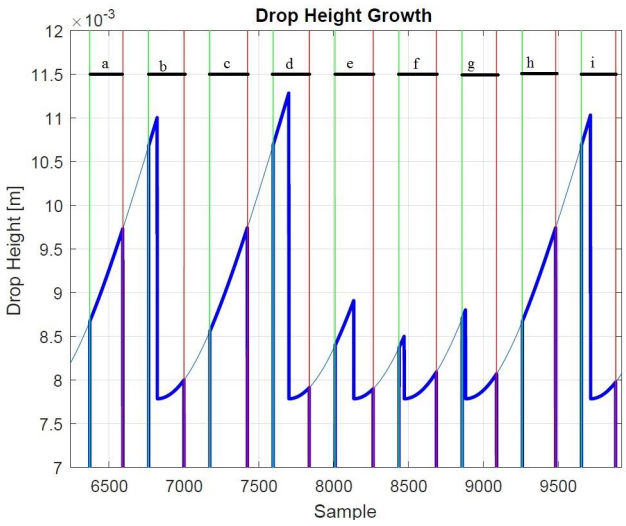

Fig. 7. Simulation of droplet height for the pulses from a to i.

$U_{line}(T) = \alpha \cdot T + \beta$, where α and β are constants. The error is found as

$$Error = \sum_{i=T_4}^{T_{end}} (U_m(i) - \alpha \cdot T(i) - \beta)^2 \qquad (6)$$

After time T_{end} this Error can be calculated.

To improve the observer another criteria is incorporated. Looking at Fig. 8 a spike can bee seen in the interval from T_4 to T_{end} in pulse number 19 and 22. From a long time series this phenomena is never observed when no detachment.

Using a high-pass filter a potential spike is identified

$$\Delta U_m(i) = -a\Delta U_m(i-1) + b(U_m(i) - U_m(i-1)) \qquad (7)$$

here ΔU_m is the hight-pass filtered version of U_m, a, b are constants. The $\Delta U_{m,max}$ is compared to a threshold to find spikes. The final observer combines the two criteria.

V. Test Results for Observer

For all tests the weldings are performed with the Migatronic process 112, at 100 [A]. This gives a wire feed rate of 5.0 [m/min] and a workpiece of 3 mm thickness.

A voltage sequence U_m from 28 current pulses I_{ref} can be seen in Fig. 8. From camera it is identified where detachments take place, if detachment the voltage curve is black and for no detachment the curve is red. Furthermore the straight lines from T_4 to T_{end} are indicated (green).

The cross correlation between the measured voltage and the straight line is seen in Fig. 9 where black is pulses with detachment and blue pulses without detachment; furthermore the spike criteria is shown with a red star. The spike criteria

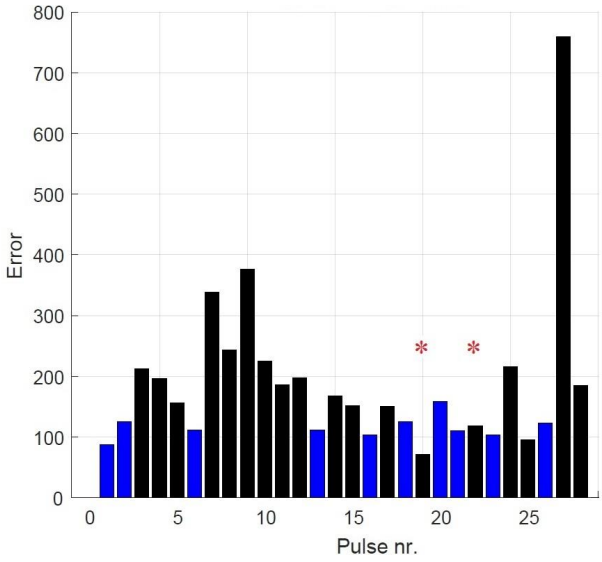

Fig. 9. Cross-correlation between the green line and the curvature for the 28 pulses. Detachment black. No detachment blue. Spikes indicated by red stars at pulse number 19 and number 22.

bypasses the shape criteria. As seen there is a error level (threshold) nearly separating the two outcomes. For a longer time series of 90 pulses the combined criteria gave correct answer for 84 pulses equivalent to 93 %.

VI. AUTOMATIC WELDING PARAMETER ADJUSTMENT BASED ON THE OBSERVER

One of the uses of the droplet observer is to adjust the welding pulse shape.

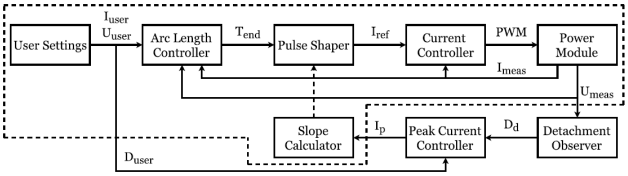

Fig. 10. Concept for automatic parameter adjustment. The old controller is in the dotted line.

In Fig. 10 a control concept for automatic adjustment of I_{ref} is shown. The two boxes 'Detachment Observer' and 'Peak Current Controller' are added to the original controller.

Detachment of all droplets requires a high peak welding current however this may cause problems as the welding pool will reach a high temperature resulting in a poor welding. A compromise could be to allow few non-detached droplets. This may be achieved by a reference number of non-detachments per N pulses, the observer calculates the non-detachments for the same N pulses. The error is feed into a PI controller that may increase/decrease the current level, [10], [11].

Using this new control set-up simple tests have been made where the maximum level of the current pulse has been

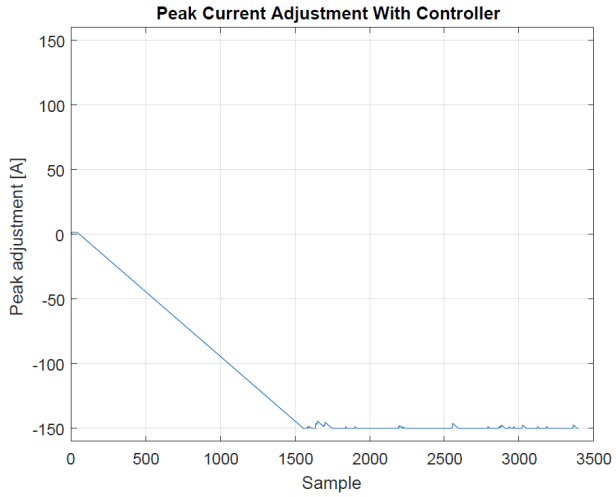

Fig. 11. Automatic adjustment of current starting at a high current level.

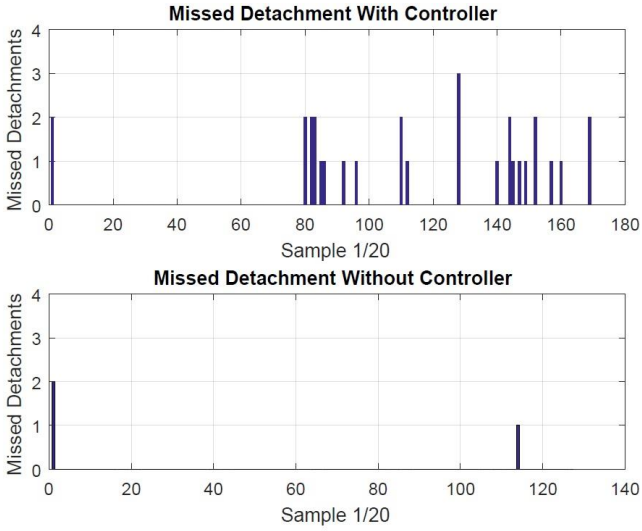

Fig. 12. Missed detachments with the new controller (top plot) and the traditional controller in the bottom plot. On the x-axis each number represents an addition of 20 samples. The y-axis is the sum of missed detachments.

adjusted to give an acceptable number of no-detachments per 20 pulses.

In Fig. 11 the welding current is pre-set to a high value I_{ref}. The controller reduces the current until the reference number of errors occur. In Fig. 12 the missed detachment per 20 pulses is shown in the top-plot, the bottom plot shows the missed detachments with the initial high current.

In Fig. 13 the welding current is starting at a low reference current I_{ref} resulting in too many no-detached droplets as seen in the upper plot Fig. 14. First the controller has adjusted the current upwards resulting in all droplets are detached (overshoot); after 2000 samples the current is fine tuned to give the reference number of no-detachments. The bottom plot in Fig. 14 is the missed detachments using the initial low I_{ref} without the new controller.

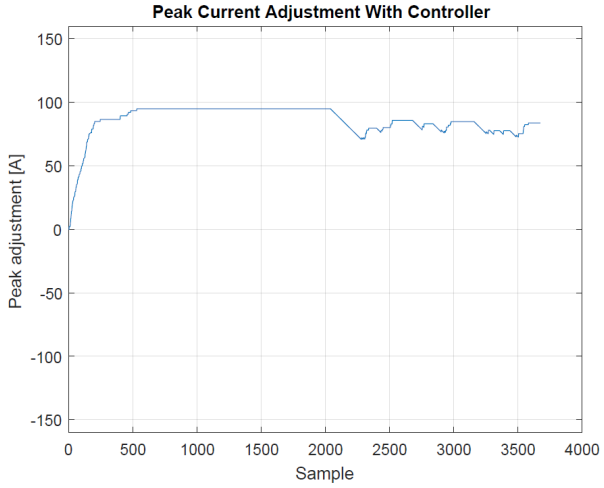

Fig. 13. Automatic adjustment of current starting at a low current level.

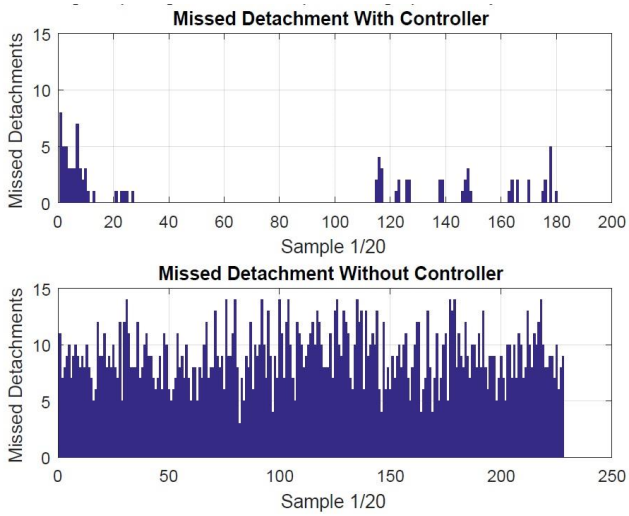

Fig. 14. Missed detachments with the new controller (top plot) and the traditional controller in the bottom plot. On the x-axis each number represents an addition of 20 samples. The y-axis is the sum of missed detachments.

VII. CONCLUSIONS

In this paper a new method for observing droplet detachment from a GMAW is described. The method is based on simple correlation analysis between a part of the voltage curvature and a straight line combined with a spike detection implemented as a high pass filter and a comparator. The simplicity of the observer facilitate real time implementation on an embedded welding computer. The observer has a success rate of 93%. An application of the observer shows it ability to automatic adjust the welding current to obtain few non-detachment of droplets. Until now the observer has only been tested on one type of welding thread and the designed controller was only used for proof of concept. Future work will clarify the applicability of the work.

ACKNOWLEDGMENT

The authors would like to thank Jesper L. Skovfo and Mads Jensen Migatronic A/S for valuable comments and advice.

REFERENCES

[1] J. S. Thomsen. Advanced Control Methods for Optimizing of Arc Welding. *PhD thesis*, Aalborg University, Denmark, August 2004.
[2] S. K. Gammeljord. Observation and Control Strategy of One Droplet Per Pulse. *Master thesis*. Aalborg University, Denmark, June 2017.
[3] M. Boselli, V. Colombo, E. Ghedini, M. Gherardi and P. Sanibondi. Dynamic analysis of doplet transfer in gas-metal arc welding: modelling and experiments. *Neural Plasma Sources Science and Technology*, Vol. 21, No. 5, 2012.
[4] J.F. Lancaster. The Physics of Welding. *Physics in Technology*, Vol. 15, 1984.
[5] Z. Bingul and G.E. Cook. Dynamic Modeling of GMAW Process. *Proc. Int. Con. on Robotics and Automation*, Detroit Michigan, USA, 1999.
[6] K.L.Moore, D.S.Naidu, R.Yender and J.Tyler. Gas metal arc welding control: Part I: Modeling and Analysis. *Nonlinear analysis, Theory, Methods and Applications*, Vol. 30, No. 5 pp 3101 – 3111, 1997.
[7] F. Wang, W.K. Hou, S.J. Hu, E. Kannatey-Asibu, W. W. Schultz and P.C. Wang. Modelling and analysis of metal transfer in gas metal arc welding. *Journal of physics D: Applied Phys.*, Vol. 36, pp 1143 – 1152, 2003.
[8] M. Jensen, R. Pedersen and J.J. Petersen. Melting Rate estimation and Control for Gas Metal Arc Welding. *Master thesis*, Aalborg University, Department Automation and Control, 2010.
[9] J.P. Planckaert, E.H. Djermoune, D. Brie, F. Briand and F. Richard. Modeling of MIG/MAG welding with experimental validation using an active contour algorithm applied on high speed movies. *Applied Mathematical Modelling*, Vol. 34, pp 1004 – 1020, 2010.
[10] G.F. Franklin, J. D. Powell and A. Emami–Naeini. Feedback Control of Dynamic Systems *Pearson Prentice–Hall*, 2006.
[11] K.J. Åstrøm and T. Hägglund. Advanced PID control. *ISA*, Instrumentation, Systems, and Automation Society, 2006.